T. L. Naing, J. N. Nilchi, R. Liu, T. O. Rocheleau, and C. T.-C. Nguyen, "Active *Q*-control for improved insertion loss micromechanical filters," *Proceedings*, IEEE Int. Frequency Control Symp., Taipei, Taiwan, May 19-22, 2014, pp. 612-617.

Active *Q*-Control for Improved Insertion Loss Micromechanical Filters

Thura Lin Naing, Jalal Naghsh Nilchi, Ruonan Liu, Tristan O. Rocheleau, and Clark T.-C. Nguyen
Dept. of Electrical Engineering and Computer Sciences
University of California at Berkeley
Berkeley, CA 94720 USA
E-mail: thura@eecs.berkeley.edu

***Abstract*—The use of active feedback in closed-loop with two electrodes of a four-electrode capacitive-gap transduced wine-glass disk resonator has enabled boosting of the effective resonator *Q* and independent control of insertion loss across the two other electrodes. To demonstrate the utility of this approach, two such *Q*-boosted resonators wired as a parallel-type micromechanical filter achieve a tiny 0.001% bandwidth passband centered around 61 MHz with only 2.7 dB of insertion loss—something not possible with the intrinsic resonator *Q* of 57,000, but quite possible with *Q*'s actively boosted to 670,000. In the feedback loop, the gain and phase of the active circuit are controlled to precisely add or cancel resonator damping while maintaining a suitable loop gain (i.e., less than unity if the feedback is positive). Unlike past kHz-frequency efforts, the split electrode design used here removes the amplifier feedback loop from the signal path allowing independent control of input-output coupling, *Q*, and frequency, the last of which comes about via either electrical stiffness changes or intentional changes in active circuit phase shift. The ability of this scheme to both raise and decrease resonator *Q* not only allows creation of narrow channel-select filters with insertion loss lower than otherwise achievable with un-boosted *Q*'s, but also opens the possibility of maximizing the dynamic range of a communication front-end without the need for a variable gain LNA.**

Keywords*— *MEMS, filter, active-Q control, micromechanical, wine-glass disk, low insertion loss, resonator, RF MEMS.

I. Introduction

The increasing role of wireless technology in our daily lives is accompanied by a need for reduced radio power consumption. This will be especially important as wireless devices become ubiquitous, going beyond the smartphones of today to perhaps networks of more than a trillion autonomous sensors of tomorrow [1]—sensors for which no one wants to replace batteries. Among components in a typical radio receiver, the front-end filters play a pivotal role in reducing power consumption. In particular, by removing unwanted blockers before they reach front-end electronics, these filters allow said electronics to operate with substantially lower dynamic range than would otherwise be needed, hence, substantially lower power consumption.

From this perspective, the high-*Q* SAW and FBAR vibrating mechanical devices that make up today's RF bandpass filters are already responsible for significant power savings in wireless handsets. Indeed, their *Q*'s in the low thousands make possible 3% bandwidth filters that reject potentially large out-of-band interferers immediately after the antenna, allowing for significant LNA and mixer dynamic range

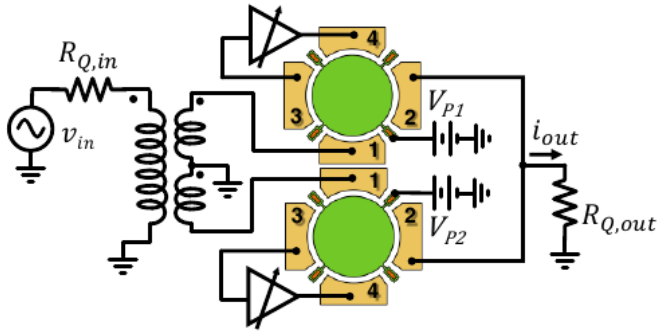

Fig. 1: *Q*-boosted parallel filter comprised of two independent wine-glass disk resonator and amplifier circuits, all in a typical measurement circuit. Here, the filter input is driven differentially while output currents are combined to generate the response of Fig. 6.

reductions. Still, there is room for improvement. In particular, although good enough to select a frequency *band* of *many* channels, the *Q*'s attainable by commercial resonator technology are not sufficient to realize filters with bandwidths small enough to select *single channels*. If possible, such a capability would allow removal of not only out-of-band interferers, but also in-band ones. This would then provide several orders more reduction in power consumption, not just from reduced dynamic range, but also due to the availability of much more efficient receiver architectures when there are no interferers [2].

Unfortunately, the resonator *Q* required for such a channel-selecting filter is quite daunting. For example, a 400-kHz bandwidth filter designed to select a single 200-kHz wide GSM-850 channel (and reject all others) would need constituent resonators with *Q*'s greater than 15,000 to maintain less than 2 dB of insertion loss (I.L) [3]. Along similar lines, sensor network nodes with much smaller data transfer needs might benefit from even smaller channel bandwidths, on the order of only a few kHz, which at 433 MHz would represent only 0.002% bandwidth, for which resonator *Q*'s on the order of 370,000 would be required!

Pursuant to achieving such *Q*'s for filters, this work explores the use of active positive feedback to boost the *Q*'s of the constituent passive resonators in a parallel-class filter and thereby make possible sub-0.01% bandwidth and its associated radio power savings for sensor network nodes. Specifically, the use of active feedback in closed-loop with two electrodes of a four-electrode capacitive-gap transduced wine-glass disk resonator has enabled boosting of the effective resonator *Q* and independent control of insertion loss across the

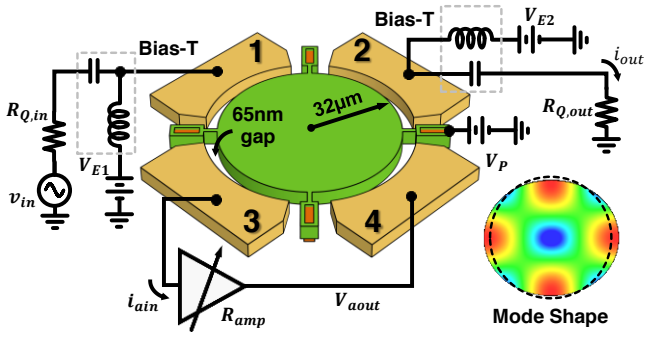

Fig. 2: Circuit schematic of an active *Q*-controlled resonator. A transimpedance amplifier provides closed-loop feedback using two electrodes of a wine-glass resonator, while the remaining two electrodes serve as input/output.

two other electrodes. As a first demonstration of the capability of this approach, two such *Q*-boosted resonators wired in the parallel-type micromechanical filter [4] of Fig. 1,achieve a tiny 0.001% bandwidth passband centered around 61 MHz with only 2.7 dB of insertion loss—something not possible with the intrinsic resonator *Q* of 60,000, but quite possible with *Q*'s actively boosted to 670,000. Unlike past efforts [5, 6] operating at kHz-frequencies, the split electrode design used here removes the amplifier feedback loop from the signal path allowing independent control of input-output coupling, *Q*, and frequency.

II. *Q* and Insertion Loss Adjustable Resonator

Fig. 2 presents details of the *Q*-boosted resonator sub-circuit used twice in the filter circuit of Fig. 1. This sub-circuit essentially combines a wine-glass disk resonator with a gain and phase-controllable Trans-Impedance Amplifier (TIA). The wine-glass disk comprises a 2 μm-thick, 32 μm-radius polysilicon disk supported at quasi nodal points by four beams and surrounded by electrodes spaced only 65 nm from its edges. To excite the resonator into motion, a bias voltage V_P is applied to the disk and an ac drive voltage to the input electrode. These voltages combine to produce a force across the input electrode-to-resonator gap that at resonance can excite the wine-glass (i.e., compound (2, 1)) vibrational mode shape, shown in Fig. 2, which comprises expansion and contraction of the disk along orthogonal axes. The expression for resonance frequency takes the form [7]

$$f_{nom} = \frac{K}{R}\sqrt{\frac{E}{\rho(2+2\sigma)}} \qquad (1)$$

where *R* is the disk radius, *K* = 0.373 for polysilicon structural material, and *E*, *σ*, and *ρ* are the Young's modulus, Poisson ratio, and density of the structural material, respectively.

Once vibration ensues, voltages across the electrode-to-resonator gaps generate currents that then serve as electrical input/output (I/O) signals at ports 1 and 2 respectively; and as feedback control signals at ports 3 and 4 conditioned by the TIA connected to these ports.

In the hookup of Fig. 2, the transresistance gain of the TIA adds or subtracts from the damping of the resonator to yield a total effective damping (and thus, *Q*) controllable up or down via the gain and phase of the TIA. If the TIA gain and phase are configured to realize positive feedback with loop gain less than unity, then from I/O terminals 1 and 2 the device looks like an electrical resonator sporting a bandpass biquad transfer function like any other electrical resonator, except with extremely high *Q* on the order of millions. As such, its small-signal circuit model derives principally from a core *LCR* tank.

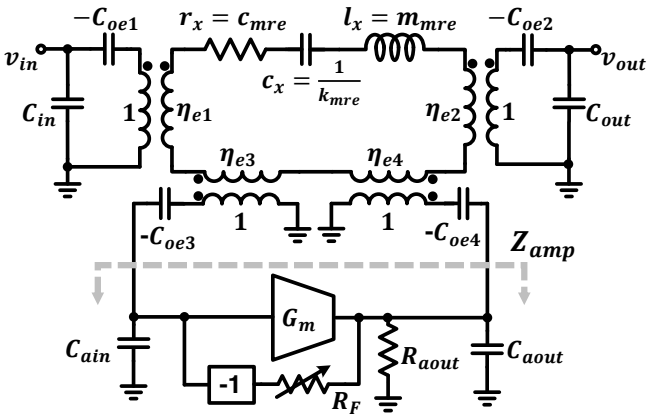

Fig. 3: Equivalent small signal circuit model for the *Q* and insertion loss adjustable resonator of Fig. 2, with electrodes 1-2 used for input and output and electrodes 3-4 embedded in a feedback loop with the amplifier to enable control of *Q*.

A. Resonator-Amplifier Electrical Model

To help quantify the *Q* attainable, Fig. 3 shows the complete small signal model of the Fig. 2 hookup, using the multiport negative capacitance resonator equivalent circuit from [8]. Here, C_{in}, C_{out}, C_{ain}, and C_{aout} represent capacitance derived from both intrinsic electrode-to-resonator capacitors; and from parasitic capacitors surrounding the resonator structure, e.g., from bond pads. In the resonator model, the values of the core *LCR* are [9]:

$$r_x = c_{mre}, \quad l_x = m_{mre}, \quad c_x = 1/k_{mre} \qquad (2)$$

where c_{mre}, m_{mre}, and k_{mre} are the mechanical damping, mass, and stiffness of the resonator, respectively, determined via equations given in [10]. The four capacitive-gap electrodes in Fig. 2 equate to four negative capacitor-transformer pairs [8], with element values

$$C_{oen} = \frac{\varepsilon_0 A_{on}}{d_o} \quad and \quad \eta_{en} = V_{PEn}\frac{\partial C}{\partial r} \qquad (3)$$

where A_{on} is the static electrode-to-resonator overlap area of the n^{th} electrode, d_o is the electrode-to-resonator gap spacing (assumed the same for all electrodes), $\partial C/\partial r$ is the change in resonator-to-electrode capacitance per unit radial displacement, and V_{PEn} is the DC voltage across the gap of the n^{th} electrode: for instance, $V_{PE1} = V_P - V_{E1}$ for electrode 1 in Fig. 2.

Connecting a Trans-Impedance Amplifier (TIA) with transconductance G_m and output resistance R_{aout}, in negative shunt-shunt feedback through R_F gives a total impedance looking into the amplifier of

$$Z_{amp} = \frac{-R_F A_v \omega_{in}\omega_{out}}{s^2 + (\omega_{in}+\omega_{out})s + \omega_{in}\omega_{out}(1+A_v)} \qquad (4)$$

where

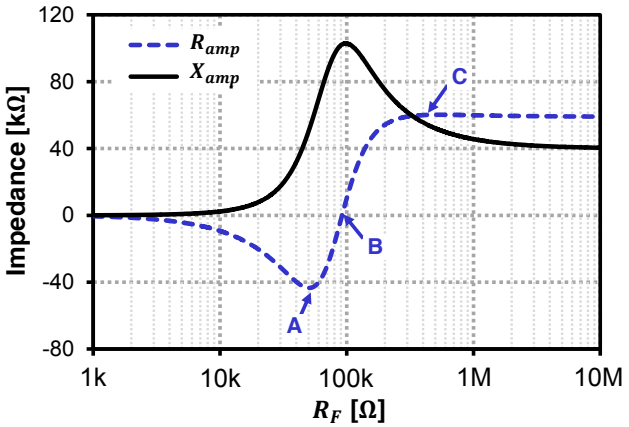

Fig. 4: Theoretical prediction of resistance (dotted blue) and reactance (black) parts of the impedance, Z_{amp}, looking into the TIA amplifier as the feedback resistor, R_F, increases. Here, approximate resistance and capacitance values for the amplifier in this work are used for simulation.

$$\omega_{in} = \frac{1}{R_F C_{ain}},\ \omega_{out} = \frac{1}{(R_F \,//\, R_{aout})C_{aout}} \qquad (5)$$
$$A_v = G_m(R_F \,//\, R_{aout})$$

Fig. 4 plots Z_{amp}'s resistance, R_{amp}, and its reactance, X_{amp}, as the feedback resistor R_F of the TIA changes. Only the real (resistive) part of Z_{amp} influences the total effective damping of the resonator, which with this influence becomes

$$c_{eff} = c_{mre} + R_{amp}\eta_{e3}\eta_{e4} \qquad (6)$$

The resultant effective Q then takes the form

$$Q_{eff} = \frac{k_{mre}}{\omega_o c_{eff}} \qquad (7)$$

which is directly controllable (up or down) via R_F. Clearly, Q_{eff} is larger than the intrinsic Q of the device when R_{amp} is negative and Q_{eff} is smaller when R_{amp} is positive, and the transition occurs (point B in Fig. 4) when

$$R_F = \frac{G_m}{C_{in}C_{out}\omega_o{}^2} \qquad (8)$$

The maximum Q_{eff} occurs at point A in Fig. 4, while the minimum occurs at point C. It is important to note that c_{eff} must be greater than zero for the system to be stable. This means that the loop gain, T, of the feedback loop must satisfy:

$$T = \frac{-R_{amp,min}}{R_{x34}} = \frac{-R_{amp,min}}{c_{mre}/\eta_{e3}\eta_{e4}} = 1 - \frac{Q_{int}}{Q_{eff}} < 1 \qquad (9)$$

where R_{x34} is the motional impedance looking into electrodes 3 and 4, and Q_{int} is the intrinsic Q of the resonator. In practice, the loop gain T should not be too close to unity, lest some unexpected variation, e.g., noise, acceleration, bumps it past 1, after which oscillation ensues. Thus, stability considerations will likely limit the amount of Q-boost in practical design to less than 100 times.

B. Amplifier-Derived Frequency-Pulling

During operation, the gap spacing between resonator and electrode changes, which in turn generates a changing electric field, and hence varying electrostatic force in the gap. In a small-signal model, this force is in phase and proportional

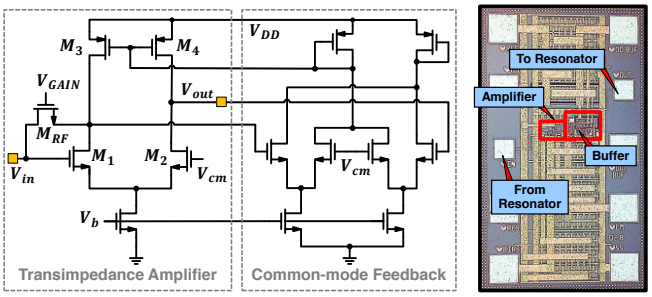

Fig. 5: (a) Transimpedance Amplifier circuit comprising a fully differential CMOS amplifier with one end connected in shunt-shunt feedback, and output taken from the other end to realize a 0° input-output phase shift. Transistor M_{RF} serves as a voltage controllable shunt-shunt feed-back resistor, allowing easy adjustment of TIA gain via its gate voltage V_{GAIN}. (b) Die photo of the fabricated amplifier ASIC.

to disk edge displacement, and thus meets the definition of stiffness. Popularly termed electrical stiffness, this "softens" the equivalent stiffness of the resonator resulting in a negative shift in the resonance frequency [11]. The resultant electrical stiffness generated from the gaps at electrodes 3-4 is:

$$k_{e34} = \eta_{e3}\eta_{e4}\left[\frac{1}{C_{oe3}} + \frac{1}{C_{oe4}} + \omega_o X_{amp}\right] \qquad (10)$$

which subtracts from the resonator's mechanical stiffness to yield a resonance frequency given by

$$f_o = f_{nom}\sqrt{\left[1 - \frac{k_{e1} + k_{e2} + k_{e34}}{k_{mre}}\right]} \qquad (11)$$

where k_{e1} and k_{e2} are the effective electrical stiffnesses from the gap at electrode 1 and 2, respectively.

C. Transimpedance Amplifier Design

Shown in Fig. 5(a), the transimpedance amplifier is similar to that used in [12] and consists of a fully differential CMOS amplifier connected in shunt-shunt feedback on one side, with output taken from the other side to realize a 0° phase shift from input to output. Transistors, M_1-M_4, comprise the basic differential pair biased by a common-mode feedback (CMFB) circuit that preserves low output resistance and cancels out common-mode noise, including that caused by vibration. The action of CMFB symmetrically balances the differential pair circuit, allowing the use of a half circuit to analyze it. Doing so yields a transconductance gain (G_m) of $0.5g_{m1}$and output resistance (R_{aout}) of approximately $r_{o2}//r_{o4}$, where g_m and r_o are transconductance and output resistance of a transistor respectively as defined in [13].The MOS transistor M_{RF} is biased in the triode region to serve as a voltage controllable shunt-shunt feedback resistor (R_F) that allows convenient adjustment of the TIA gain via its gate voltage, V_{GAIN}.

The amplifier IC was fabricated in a 0.35 µm CMOS technology. Although the entire die, shown in Fig. 5(b), occupies an area of 900µm×500µm, the actual sustaining amplifier only consumes about 60µm×60µm. The rest of the area is consumed by 1) an on-chip buffer used to drive 50 Ω measurement systems; 2) by-pass capacitors that further reduce noise on DC supply lines; and 3) bond pads.

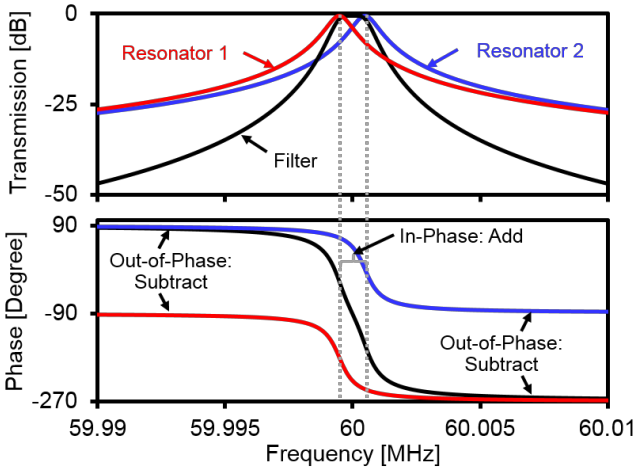

Fig. 6: Description of parallel filter operation, where two differentially driven bandpass biquad responses add to form a flat passband (between the peaks) and subtract in the stopband (outside the peaks) to provide greater stopband rejection.

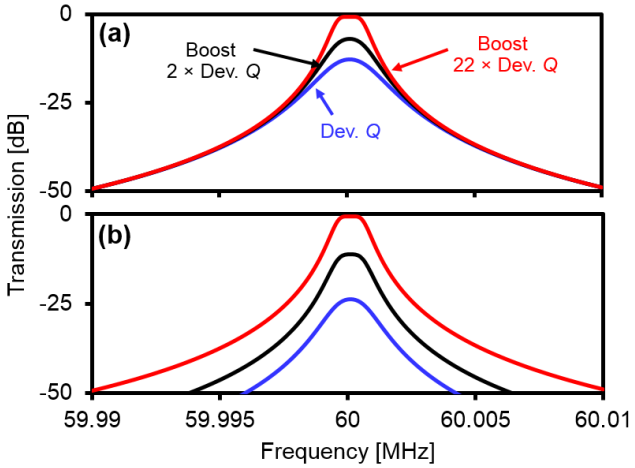

Fig. 7: Simulated parallel filter responses for a narrow 0.002% bandwidth filter with low Q (intrinsic device's Q) equivalent to $1.36 \times BW_{fil}$ (blue), Q-boosted by two times (black), and Q-boosted by 22 times (red). (a) shows responses for constant R_Q (its value is the needed R_Q for highest Q case) and IL improvement of 12 dB. (b) illustrates that the filter can be terminated properly by adjusting the bias voltage across input and output gaps while R_Q is kept constant. Boosting Q by 22 times improves IL by 23 dB. Note that the Q equivalent to $1.36 \times BW_{fil}$ (blue case) is too small for the filter to be terminated properly.

III. Active Q-Boosted Filter Implementation

To create a filter response, the circuit of Fig. 1 combines into a parallel-class filter similar to that of [4]: two Fig. 2 electromechanical circuits with resonance frequencies spaced from one another by the desired passband bandwidth. A balun converts a single ended input at the left into a differential drive signal with plus end applied to one resonator input and minus to the other, so that each resonator receives oppositely phased inputs. The output terminals of each device are then tied together so that their output currents add.

This filter operates as illustrated in Fig. 6, which plots the individual resonator spectra together with the resulting filter spectrum. As shown, differential drive of the resonators produces a relative phase shift of approximately 0° between the resonator peaks, which allows their outputs to add to form a flat filter passband between these peaks. Meanwhile, outside the passband the resonators vibrate 180° out-of-phase, giving rise to subtraction that steepens the roll-off to the stopband.

A. Adjustable Dynamic Range

As with any bandpass filter, the higher the Q of the constituent resonators, the lower the insertion loss. This means the insertion loss of the filter should be fully controllable by merely adjusting the gain of the Q-controlling amplifiers placed in feedback between terminals 3 and 4 of each resonator. Doing so when simulating the Fig. 1 equivalent circuit for a 60-MHz, 0.002%-bandwidth two-resonator filter for a constant termination impedance, without adjusting dc-bias to re-match the terminations, yields the curves of Fig. 7(a), which clearly show the dependence of insertion loss on Q-controlling amplifier gain. In effect, active Q-control not only makes possible low insertion loss even for 0.002% bandwidth filters that would not be feasible otherwise; but also enables variable gain filters, as opposed to the variable gain LNA's commonly used in RF front-ends.

The curves in Fig. 7(a) lose their passband shape as Q is lowered, mainly because the motional resistance of the constituent resonators changes with their Q, so the R_Q's no longer present the needed termination. To remedy this, the electrode-to-resonator dc-bias voltages V_{PE1} and V_{PE2} can be adjusted to compensate, which then yields the curves of Fig. 7(b), where the filter frequency response retains its shape as insertion loss increases.

The ability to tune insertion loss essentially amounts to an ability to adjust dynamic range. In particular, if the input to the filter receives a signal hot enough to drive it into nonlinear behavior, one need only tune the Q-controlling amplifier gain to increase insertion loss, thereby allowing reception of the signal without desensitization. In effect, this adjustable insertion loss provides an effective bias shift for dynamic range—a very useful function for any transceiver front-end.

B. Power Consumption Considerations

The use of active circuits in an otherwise passive filter implementation does introduce power consumption, where there was none before. The extra active circuits are justified only if their presence offers performance benefits beyond what might be achieved by raising power consumption elsewhere in the system, e.g., in the LNA and/or IF channel-select filter (if realized using transistors). In fact, a typical LNA power consumption is on the order of 5 mW [14], which is needed mainly to insure adequate noise figure. Recent developments in passive transformer coupled front-ends have successfully reduced the power consumption in the LNA and mixer close to zero, but due to the lack of RF channel-select filtering in traditional technologies, power on the order of 10 mW is still needed to maintain adequate linearity in the active IF channel-select filter [15].

Meanwhile, the power required for the active circuits in the Q-boosting loop of Fig. 2 can be sub-100 μW [16, 17], making the Q-boosted MEMS approach more desirable. This point amplifies with the recognition that the loss of an RF front-end filter directly adds to the noise figure of a receiver,

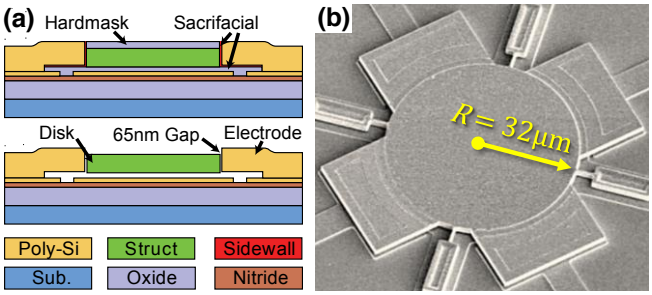

Fig. 8: (a) Cross-sections of the wine-glass disk immediately before release and after release. (b) SEM of a fabricated disk resonator device.

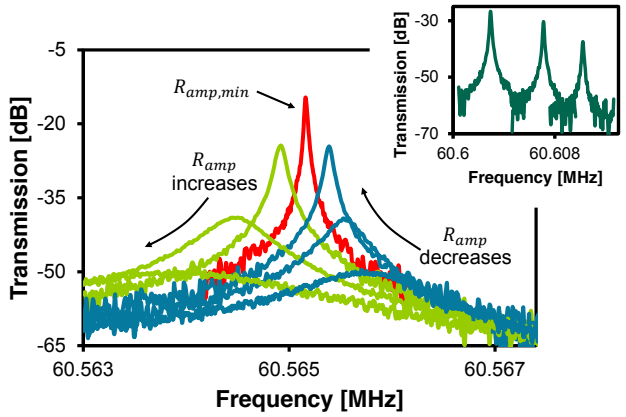

Fig. 9: Single resonator Q-boosting as a function of amplifier gain with constant V_P=8.5 V. As V_{GAIN} is decreased amplifier gain increases, boosting effective resonator Q (blue curves) from an initial intrinsic Q=57,000 to a maximum boosted Q of 2.3 million (red). On the other hand, decreasing V_{GAIN} further allows control of amplifier phase shift, leading to negative feedback and allowing controlled loading of Q (green curves). The inset demonstrates independent tuning of frequency and insertion loss via control of the voltage across input-output electrode-disk gap, all while holding Q constant by holding V_{GAIN} constant.

so lowering RF filter insertion loss by several dB is often a better investment of consumed power than lowering the noise figure of an LNA by a smaller dB number.

IV. Experimental Results

To experimentally verify the utility of active Q-boosting, wine-glass disks were designed and fabricated using a process similar to that of [18] and summarized in the cross sections of Fig. 8(a). Here, doped polysilicon serves as the structural material for resonator and electrodes, alike, and the gaps between them were set to 65 nm by a sacrificial high-temperature oxide spacer that is removed in the final release step. The process differs from previous ones in that it removes electrode overhangs via CMP—a step that improves the reliability of devices under larger dc-bias voltages. Fig. 8(b) presents the SEM of a fabricated device following release in 49% HF. With a radius of 32 μm, electrode-to-resonator gap spacing of 65 nm, and dc-bias voltage V_P of 10 V, this fabricated device provides a coupling strength of (C_x/C_o) ~0.04% at an operating frequency of 61 MHz, sufficient for the 0.001% bandwidth filter demonstrated here.

Fig. 9 presents measured electrical transmission plots for a 50 Ω-terminated single disk in a Q-controlling hookup (*cf.* Fig. 2) as a function of TIA gain and phase shift. Here, insertion loss and Q are quite tunable, with effective Q adjustable anywhere from 24k to 2.3M. Even operating at the maximum boosted Q of 2.3M, the active resonator remained stable for hours of measurement time with no evidence of oscillation, likely a result of compact implementation made possible by die-level ASIC and MEMS resonator connections. Fig. 9 also confirms that the resonance frequency shifts to the left with decreasing V_{GAIN}, as predicted by (11). The inset figure further demonstrates insertion loss tuning while maintaining constant Q (by keeping V_{GAIN} constant) via independent tuning of the input-output electrode to disk bias voltage, i.e., tuning V_{E1} and V_{E2}.

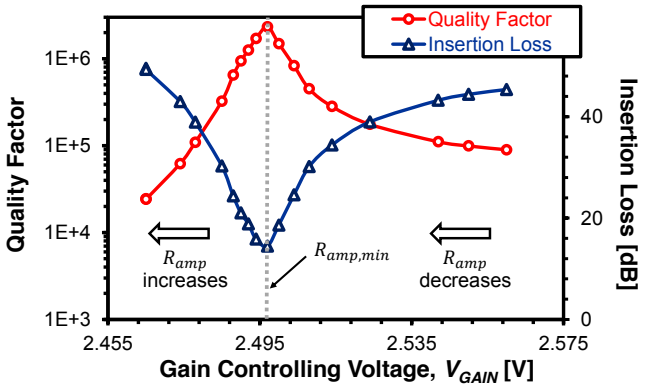

Fig. 10: Measured effective quality factor (red) and insertion loss (blue) of the resonator with constant V_P=8.5 V as V_{GAIN} of the amplifier changes.

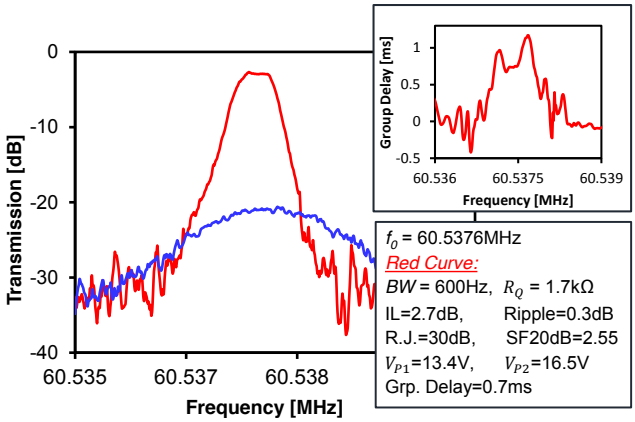

Fig. 11: Measured transmission for a two-resonator filter hooked up as in Fig. 1 and terminated by the designed (i.e., required) value of 1.7 kΩ at both input and output for the cases with (red) and without (blue) Q-boosting TIA's.

To verify the theoretical predictions of Fig. 4, Fig. 10 additionally demonstrates the Q enhancement and subsequent improvement in insertion loss when measured with 50 Ω terminations as a function of V_{GAIN} applied to the amplifier. As V_{GAIN} decreases, the shunt-shunt feedback resistance R_F in the TIA increases. As depicted in Fig. 4, with increasing R_F, R_{amp} (initially a negative value and hence boosting Q) decreases to a minimum value for the maximum Q of 2.3M and the maximum loop gain of 0.975. Decreasing V_{GAIN} further decreases Q (or increases R_{amp}) until it becomes smaller than devices' intrinsic Q at which point R_{amp} is greater than zero.

Fig. 11 finally presents the measured transmission for a

two-resonator parallel filter hooked up as in Fig. 1 and terminated by the designed (i.e., required) value of 1.7 kΩ at input and output for the cases with and without *Q*-boosting TIA's. As expected, the insertion loss is a dismal 21 dB without *Q*-boosting of the constituent resonators; compared with only 2.7 dB when the TIA's boost *Q*'s. Indeed, 2.7 dB is quite impressive for a percent bandwidth this small.

On the other hand, the stopband rejection of only 30 dB seen in Fig. 11 is less than expected. The insufficient stopband rejection actually derives from the measurement apparatus and scheme, not the device itself. In particular, the current measurement simulates the needed filter terminations using network analyzer-based load simulation, rather than a real 1.7 kΩ termination impedance, and this compromises the noise floor of the instrument. An improved measurement effort using real terminations, currently underway, is expected to improve this low rejection.

V. Conclusions

The demonstration in this work of a 0.001% bandwidth micromechanical filter comprised of actively *Q*-boosted passive resonators with only 2.7 dB of insertion loss is the first of its kind on the micro-scale and presents opportunities for implementing some very unique and desired capabilities in the near future. Opportunities to realize RF channel-selecting radios were the focus of this work, and the demonstrated *Q*'s up to 2.3 million should prove very useful towards greatly lowering power consumption for the low data rate wireless communications needed for network sensors. Bandwidths as small as 0.001% might further enable noise shaping for oscillators and other applications to unprecedented performance marks.

Although this work focused on very small percent bandwidth filters, it is worthwhile to take a step back and consider use of these techniques in more mainstream applications, like cellular communications, for which RF channel-selection still offers substantial reductions in power consumption. As mentioned, existing resonator technologies do not yet possess the simultaneous *Q* and coupling to realize such a front-end. As described in this paper, as long as the small additional power consumption is acceptable, active *Q*-boosting might be a good answer for resonators that possess adequate coupling, but insufficient *Q*. In other words, RF channel-selection for piezoelectric resonators may indeed just be a few more electrodes and some active circuits away from reality, especially for piezoelectric resonators that start with decent *Q*'s, e.g., ones using capacitive-piezo transducers [19], or composite material structures [20]. This is a topic for future work.

Acknowledgement: This work was supported by grants from DARPA.

References

[1] J. M. Rabaey, J. Ammer, T. Karalar, S. Li, B. Otis, M. Sheets and T. Tuan, "PicoRadios for wireless sensor networks: the next challenge in ultra-low power design," in *Digest of Tech. Papers, the 2002 IEEE Int. ISSCC*, Feb. 2002, pp.200-201.

[2] C. T.-C. Nguyen, "MEMS-based RF channel selection for true software-defined cognitive radio and low-power sensor communications," *IEEE Communications Magazine*, vol. 51, no. 4, pp. 110-119, April 2013.

[3] A. I. Zverev, Handbook of Filter Synthesis, New York: John Wiley & Sons, 1967.

[4] J. R. Clark, A.-C. Wong, and C. T.-C. Nguyen, "Parallel-resonator HF micromechanical bandpass filters," in *Digest of Technical Papers, 1997 Int. Conf. on Solid-State Sensors & Actuators (Transducers'97)*, Chicago, Illinois, Jun. 16-19, 1997, pp. 1161-1164.

[5] C. Jeong, S. Seok, B. Lee, H. Kim and K. Chun, "A study on resonant frequency and Q factor tunings for MEMS vibratory gyroscopes," *J. Micromech. Microeng.*, vol. 14, no. 11, p. 1530–1536, 2004.

[6] C. T.-C. Nguyen and R. T. Howe, "Quality factor control for micromechanical resonators," in *Technical Digest, the 1992 Int. Electron Devices Meeting*, 13-16 Dec. 1992, pp. 505-508.

[7] M. Onoe, "Contour vibrations of isotropic circular plates," *J. Acoust. Soc. Amer.*, vol. 28, no. 6, p. 1158–1162, Nov. 1956.

[8] M. Akgul, L. Wu, Z. Ren and C. T.-C. Nguyen, "A negative capacitance equivalent circuit model for parallel-plate capacitive-gap transduced micromechanical resonators," *IEEE Transactions On Ultrasonic, Ferroelectrics, and Frequency Control*, in press.

[9] F. D. Bannon III, J. R. Clark, and C. T.-C. Nguyen, "High-Q HF microelectromechanical filters," *IEEE Journal of Solid-State Circuits*, vol. 35, no. 4, pp. 512-526, Apr. 2000.

[10] Y.-W. Lin, S. Lee, S.-S. Li, Y. Xie, Z. Ren, and C. T.-C. Nguyen, "Series-resonant VHF micromechanical resonator reference oscillators," *IEEE Journal of Solid-State Circuits*, vol. 39, no. 12, pp. 2477-2491, Dec. 2004.

[11] H. C. Nathanson, W. E. Newell, R. A. Wickstrom, and J. R. Davis Jr., "The resonant gate transistor," *IEEE Transactions on Electron Devices*, vol. 14, no. 3, pp. 117- 133, Mar. 1967.

[12] T. L. Naing, T. O. Rocheleau, Z. Ren, E. Alon and C. T.-C. Nguyen, "Vibration-insensitive 61-MHz micromechanical disk reference oscillator," in *Proceedings, the 2012 IEEE Int. Frequency Control Symposium*, Baltimore, Maryland, USA, May 22-24, 2012, pp. 276-281.

[13] P. R. Gray, P. J. Hurst, S. H. Lewis and R. G. Meyer, Analysis and design of analog integrated circuits, New York: John Wiley & Sons, INC., 2001.

[14] H. Samavati, H. R. Rategh and T. H. Lee, "A 5-GHz CMOS wireless LAN receiver front end," *IEEE Journal of Solid-State Circuits*, vol. 35, no. 5, pp. 765-772, May 2000.

[15] A. Homayoun and B. Razavi, "A 5-GHz 11.6-mW CMOS receiver for IEEE 802.11a applications," in *Proceedings, the 2013 IEEE Custom Integrated Circuits Conf.*,, Sept. 22-25, 2013.

[16] A. Nelson, J. Hu, J. Kaitila, R. Ruby and B. Otis, "A 22μW, 2.0GHz FBAR oscillator," in *Proceedings, the 2011 IEEE Radio Frequency Integrated Circuits Symposium*, Jun. 5-7, 2011.

[17] T. L. Naing, T. O. Rocheleau, E. Alon and C. T.-C. Nguyen, "A 78-microwatt GSM phase noise-compliant Pierce oscillator referenced to a 61-MHz wine-glass disk resonator," in *Proceedings, the 2013 Joint UFFC, EFTF, and PFM Symposium*, Prague, Czech Republic, Jul. 21-25, 2013, pp. 562-565.

[18] M. A. Abdelmoneum, M. U. Demirci and C. T.-C. Nguyen, "Stemless wine-glass-mode disk micromechanical resonators," in *Proceedings, the 16th IEEE Int. Conf. on Micro Electro Mechanical Systems*, Kyoto, Japan, Jan. 19-23, 2003, pp. 698-701.

[19] R. A. Schneider and C. T.-C. Nguyen, "On/off switchable high-Q capacitive-piezoelectric AlN resonators," in *Proceedings, the 27th IEEE Int. Conf. on Micro Electro Mechanical Systems*, San Francisco, California, USA, Jan. 26-30, 2014, pp. 1265-1268.

[20] C.-M. Lin, Y.-Y. Chen, V. V. Felmetsger, D. G. Senesky and A. P. Pisano, "AlN/3C–SiC composite plate enabling high-frequency and high- Q micromechanical resonators," *Advanced Materials*, vol. 24, no. 20, pp. 2722-2727, May 2012.